Preprints of the Fourth International
Symposium on Experimental Robotics, ISER'95
Stanford, California, June 30-July 2, 1995

Experimental Approach on Artificial Active Antenna

Makoto Kaneko Naoki Kanayama Toshio Tsuji

Industrial and Systems Engineering
Hiroshima University
Higashi-Hiroshima 739, JAPAN

Abstract

This paper discusses an artificial Active Antenna that can detect the contact location between an insensitive flexible beam and a 3D environment through the measurement of the rotational compliance of the beam in contact with the environment. The lateral slip, which possibly occurs for the 3D Active Antenna, overestimates the rotational compliance, and as a result, brings a large sensing error for the localizing contact point. The goal of this paper is to find the contact point under such conditions. In the first step, we push the antenna to the environment. If a lateral slip is confirmed, the pushing direction is changed continuously until we finally avoid the development of any lateral slip. We explore how to detect a lateral slip and how to determine the new pushing direction to avoid it. We experimentally verify an algorithm which can search the contact distance, even under the appearance of a lateral slip during the first step.

1. Introduction

Active Antenna is a new sensing system enabling us to detect the contact location through the measurement of the rotational compliance of an insensitive antenna in contact with an environment. In our former work, we have shown that for a planar type Active Antenna, the contact location is a function of the rotational compliance alone, and that one active motion is necessary and sufficient for localizing the contact point irrespective to friction at the point of contact, if the straight beam is utilized [1], [2]. A big advantage of Active Antenna is that a contact point is obtained through a surprisingly simple active motion, while sophisticated active motions should be prepared for most of contact sensing to avoid a large interaction force between sensor and environment. This is because the flexibility of the antenna successfully relaxes the contact force by itself, even under a large positional error.

In the 2D Active Antenna, we implicitly assumed that the antenna never makes a slip in the lateral direction, while a longitudinal slip inevitably occurs to satisfy the geometrical relationship between the antenna shapes before and after a bending deformation. The lateral slip (see Fig.1), which is the inherent characteristic for 3D Active Antenna [3], strongly depends on the direction of pushing, the friction at the point of contact, and the normal surface of the environment where the antenna makes contact. Generally, such a lateral slip overestimates the rotational compliance of the antenna which is in contact with the environment, and as a result, deteriorates the sensing accuracy directly, while the longitudinal slip brings a minor error only. In this paper, we discuss an algorithm which can detect the contact distance with a sufficient accuracy, even under the appearance of a lateral slip during the first step.

2. Related Works

A simple flexible beam sensor can take the form of a short length of spring piano wire or hypodermic tubing anchored at the end. When the free end touches an external object, the wire bends. This can be sensed by a piezoelectric element or by a simple switch [4]. A more elaborate sensor is described by Wang and Will [5]. Long antennae-like whisker sensors were mounted on the SRI mobile robot, Shakey [6], and on Rodney Brook's six-legged robot insects [7]. Hirose, et. al. discussed the utilization of whisker sensors in legged robots [8]. The sensor system is composed of an electrode and a whisker whose end is fixed at the base. This sensor unit has been arranged in an array around each foot of the legged robot, Titan III, so that it can monitor the separation between each foot and the ground to allow deceleration of the foot before contact. This sensor is also conveniently used to confirm which part of the foot is in contact with the ground. Similarly shaped whiskers have been considered for legs of

the Ohio State University active suspension vehicle [9]. Russell has developed a sensor array [10] by mounting whisker sensors on a mobile robot, and succeeded in reconstructing the shape of a convex object followed by the whisker. In his work, it is assumed that the whisker tip is always in contact with the environment, and that when the whisker contacts the environment except for the tip, it is assigned to a failure mode. The major difference between previous works [4]-[10] and ours is that the Active Antenna enables us to localize a contact point between the beam and the environment, while previous works do not.

3. Basic Structure of Active Antenna and Main Assumptions

3.1. Basic structure

Fig.1 shows an overview of the 3D Active Antenna and its coordinate system, where Σ_B (or upper script "B") and Σ_s (or upper script "s") denote the base coordinate system and the sensor coordinate system, respectively. The 3D Active Antenna is composed of an insensitive flexible beam, two actuators to move the beam in 3D space, two position sensors to measure the angular displacements ϕ_1 and ϕ_2, and a two-axis moment sensor to detect moments around both x_s and z_s axes. The moment sensor is designed so that each sensing axis can intersect with the center of rotation (the origin of the sensor coordinate system). With this sensor design, we have a common moment arm y_0 for each moment axis, as shown in Fig.2. Now, let us consider the reaction force f_c. This force can be decomposed into an axial force and a non-axial force components, respectively. Since the antenna is assumed to have a sufficiently large stiffness in the longitudinal direction, we neglect the effect due to the axial force component. So, we consider the effect due to the non axial force component f_s only. We also define the sensing plane II, with the plane spanned by two unit vectors whose directions coincide with x_s and y_s. The design orientation taken for the two-axis moment sensor enables us to evaluate the direction of the contact force projected on the plane II from the outputs of the moment sensor, since f_s is parallel to the sensing plane II.

3.2. Main assumptions

For simplifying our discussions, we set the following assumptions:

Assumption 1: The antenna has equal compliance in a plane perpendicular to the longitudinal axis.

Assumption 2: The antenna deformation is small

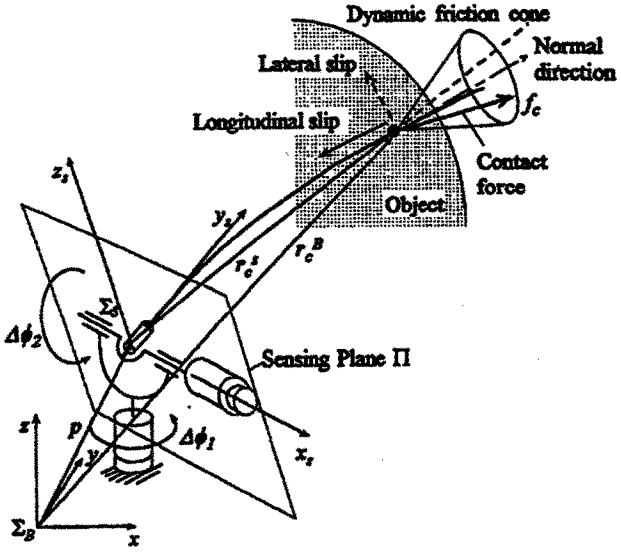

Figure 1. Basic structure and its coordinate system of 3D Active Antenna.

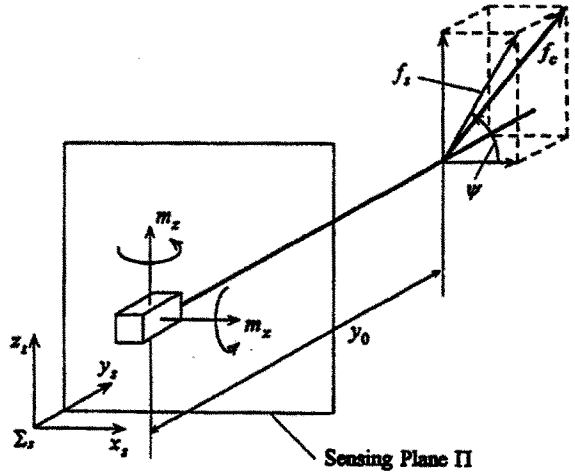

Figure 2. Sensing plane II and contact force decomposition.

enough to ensure that we can apply a linear approximation.

Assumption 3: Antenna has a sufficiently large stiffness for the axial direction to enable us to neglect the longitudinal elongation of the antenna.

Assumption 4: The compliance of the environment is sufficiently small compared with that of the antenna.

Assumption 5: Before applying an active motion, the antenna is already in contact with an environment with zero force.

4. Working Principle

4.1. Without lateral slip

In our former works [1], [2], we have shown that if there is no lateral slip, the contact distance y_0 is given

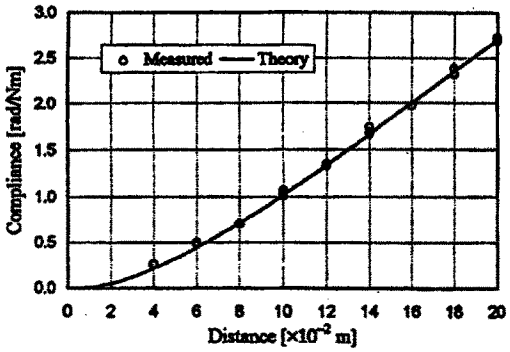

Figure 3. Calibration test without any lateral slip.

by the following equation:

$$y_0 = kc, \tag{1}$$

where k is a constant and c denotes the rotational compliance of the antenna in contact with an environment. For a beam whose cross sectional area is circular, $k = 3EI$, where E and I are Young's modulus and the second moment of cross section of the antenna, respectively. c can be computed by the torque increase and the pushing angle after the antenna makes contact with an environment. Fig.3 shows the experimental result obtained under no lateral slip, where the real line denotes the theoretical result and the circles denote experimental data for five trials. It can be seen from Fig.3 that the agreement between theoretical and experimental results is fairly good and the repeatability of experiments is also fine.

4.2. Lateral slip and its effect on contact sensing

The antenna is extremely stiff in the longitudinal direction and is a little elongated along the direction of an axial force (Assumption 3), while it easily deforms for a bending moment. When the angular displacements, $\Delta\phi_1$ and $\Delta\phi_2$, are imparted to the antenna, it deforms while keeping contact as shown in Fig.1. During this pushing motion, it continuously makes a longitudinal slip on the point of contact to the environment. This allows us to consider only the case of the dynamic friction cone during the whole active motion.

Fig.4 shows the relationship among the virtual displacement vector $\Delta r_v^{s+\Delta}$, the effective displacement vector $\Delta r_e^{s+\Delta}$ and the dynamic friction cone after a pushing motion, where α is the angle of the dynamic friction cone. Since we assume the uniform compliance by Assumption 1, the contact force always appears in the opposite direction against the effective displacement vector $\Delta r_e^{s+\Delta}$. This means that

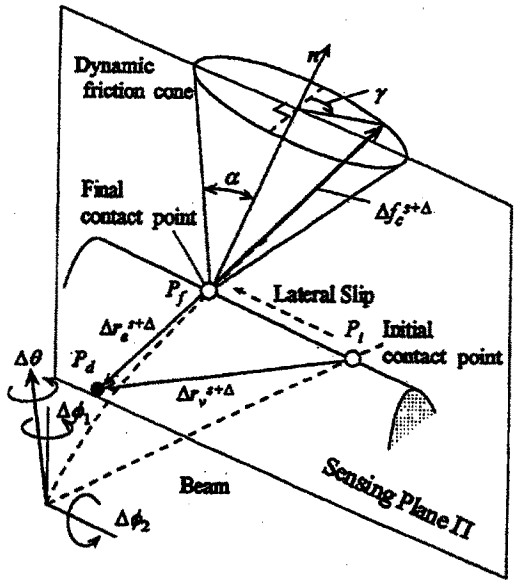

Figure 4. A general view of 3D Active Antenna when a lateral slip occurs.

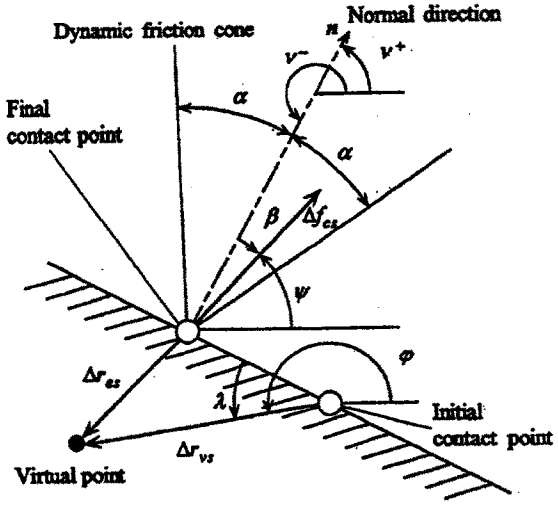

Figure 5. Notations on the sensing plane II.

the contact point moves so that $\Delta r_e^{s+\Delta}$ and $\Delta f_c^{s+\Delta}$ are colinear each other. It should be noted that the force projected on the sensing plane can exist not only on the boundary but also within the dynamic friction cone, while the contact force should always exist on the boundary of dynamic friction cone. Since $\|\Delta r_v^{s+\Delta}\| > \|\Delta r_e^{s+\Delta}\|$ while under a lateral slip, $\Delta f_c^{s+\Delta}(\|\Delta r_v^{s+\Delta}\|) > \Delta f_c^{s+\Delta}(\|\Delta r_e^{s+\Delta}\|)$, which means that the contact force under no lateral slip is larger than that under one for the same $\Delta\phi_1$ and $\Delta\phi_2$. Thus, the rotational compliance is generally overestimated under a lateral slip. As a result, the sensing accuracy will be deteriorated.

Fig.5 shows several physical parameters on the sensing plane Π, where all components are projected on the sensing plane Π, and ν^+, ν^-, φ and ψ denote outer and inner normal directions of the environment's surface, the direction of Δf_{cs}, and the pushing direction with respect to the sensor coordinate system, respectively.

4.3. Judgement of contact states

There are two physical parameters obtained by the sensors.

(1) The direction of contact force projected on Π, ψ: The moment sensor can involve the following information.

$$m_x = y_0 \|\Delta f_{cs}\| \sin\psi \tag{2}$$

$$m_z = -y_0 \|\Delta f_{cs}\| \cos\psi \tag{3}$$

By dividing each side, we obtain,

$$\tan\psi = -\frac{m_x}{m_z} \tag{4}$$

(2) The pushing direction φ:
Since each actuator has a position sensor, the pushing direction can also be measured. φ can be regarded as an input for this sensor system, and then it provides ψ as an output. Based on these informations, the sensing algorithm should be planned.

There are three patterns for judging the contact states, as shown in Fig.6, where δ is the angle expressing the difference between ψ and φ. If δ is less than π, it means that the antenna made a slip in the left direction. If δ is greater than π, it means that the antenna made a slip in the right direction. If δ is equal to π, it means that there was no slip during the pushing motion.

4.4. Sensing strategy

The main goal is to find the pushing direction avoiding any lateral slip, because once we find such a direction, the problem reduces to that of a planar Active Antenna [2], [3]. Fig.7 explains the sensing strategy eventually leading to the normal direction of environment.

1) The 1st trial:
For the first trial, the antenna is pushed toward an arbitrary direction $\varphi^{(1)}$. Let $\psi^{(1)}$ be the direction of contact force resultantly obtained by the first pushing motion. Since $\delta < \pi$ in this particular example (Fig.7), the sensor system can recognize that the antenna made a slip in the left direction.

2) The 2nd trial:
The second pushing direction is chosen so that the slip may appear in the opposite direction against the first one. This can be done by choosing the pushing direction in the following,

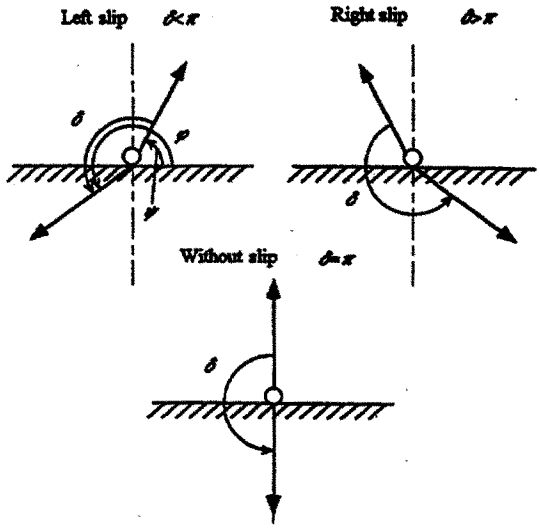

Figure 6. Three patterns of the contact states.

$$\varphi^{(2)} = \varphi^{(1)} - \mathrm{sign}(\delta^{(1)} - \pi) \cdot \frac{\pi}{2}, \tag{5}$$

where $\delta^{(1)} = \varphi^{(1)} - \psi^{(1)}$. When we choose the second pushing direction according to eq.(5), $\psi^{(1)}$ and $\psi^{(2)}$ always lie in two different regions, namely, one is the right half plane with respect to the outer normal vector, and the other is the left one. Since the contact force projected on Π can never be away from the boundary of the dynamic friction cone projected on Π, the following condition holds.

$$\nu^+ - \frac{\alpha}{2} < \frac{\psi^{(1)} + \psi^{(2)}}{2} < \nu^+ + \frac{\alpha}{2} \tag{6}$$

Eq.(6) implies that the angle between ν^+ and the arithmetic mean of $\psi^{(1)}$ and $\psi^{(2)}$ is less than $\alpha/2$.

3) The 3rd trial:
The third pushing direction is chosen so that the extended line may divide $\psi^{(1)}$ and $\psi^{(2)}$ equally, namely,

$$\varphi^{(3)} = (\psi^{(1)} + \psi^{(2)})/2 + \pi \tag{7}$$

From ineq.(6) and eq.(7), the difference between $\psi^{(3)}$ and ν^+ is at most $\alpha/2$.

4) The 4th trial:
Picking up $\psi^{(3)}$ and either $\psi^{(1)}$ or $\psi^{(2)}$, we choose the fourth pushing direction in the following.

$$\varphi^{(4)} = (\psi^{(3)} + \psi^{(1|2)})/2 + \pi \tag{8}$$

where $(a|b) \equiv \{x | \min(|\delta^{(x)} - \pi|), x = a, b\}$ By introducing this function, we can always choose the trial whose lateral slip is smaller than the other.

Trial number		Maximum force deviation angle from the normal direction
1st	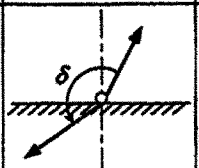	α
2nd	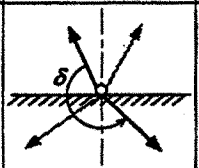	α
3rd	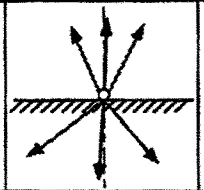	$\frac{\alpha}{2}$
4th	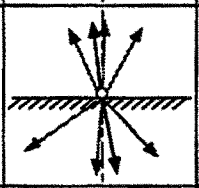	$\frac{\alpha}{2}$
n th ($n \geq 4$)		$\frac{\alpha}{2^{n-3}}$

Figure 7. Maximum force deviation angle from the normal direction for each trial.

In general, for the n-th trial ($n \geq 4$), we can easily show that the following inequality exists.

$$|\psi^{(n)} - \nu^+| < \frac{\alpha}{2^{n-3}} \quad , n \geq 4 \tag{9}$$

Since $\lim_{n\to\infty}\{\alpha/2^{n-3}\} = 0$, $\lim_{n\to\infty}\{\psi^{(n)}\} = \nu^+$, which means that the direction of contact force finally reaches the outer normal direction, namely, the pushing direction coincides with the inner normal direction. Thus, we can find the normal direction of the environment. Once we can detect the direction, the contact distance can be obtained through the pushing motion along the direction detected, because it is guaranteed that no lateral slip occurs. Thus, the convergence of the algorithm can be ensured if we impart infinite active motions to the antenna, while it is not efficient.

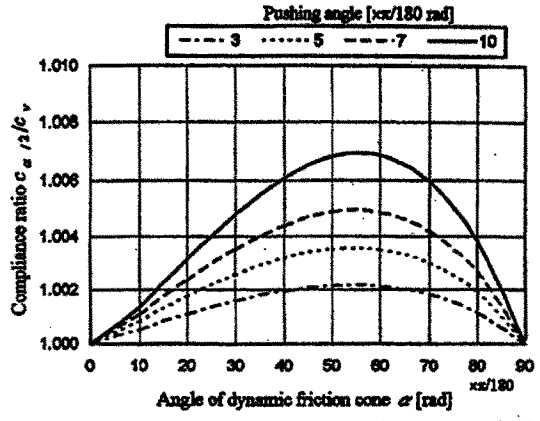

Figure 8. Compliance ratio when pushing to $\alpha/2$ from normal direction.

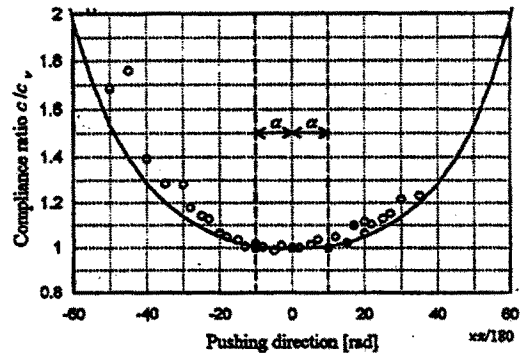

Figure 9. The relationship between c/c_ν and φ ($\alpha = \pi/18$, $\Delta\theta = \pi/36$).

4.5. When can we stop the trial?

A natural question that comes up is when we can stop the trial. In other words, how many active motions are really necessary for keeping a sufficient accuracy. Fig.8 shows the compliance ratio $c_{\alpha/2}/c_\nu$ when the pushing motion is imparted in the direction of $\alpha/2$ from ν^-, where c_ν and $c_{\alpha/2}$ denote the compliances under the pushing in ν^- and under the pushing in $\alpha/2$ from ν^-, respectively. From this figure, it can be found that if the pushing direction is selected within $\alpha/2$ from ν^-, it is ensured that the theoretical sensing error can be suppressed less than 1% irrespective to dynamic friction cone. By combining the results in Fig.7 and 8, we can say that three active motions are sufficient for keeping theoretical sensing error less than 1%.

Fig.9 shows the relationship between the pushing direction φ and compliance ratio between pushing to ν^- and pushing to φ, where the real line denotes the analytical result and the circles show the experimental results, and the angle of the dynamic friction is approximately 10 degrees. Experimental results exhibit almost unity for the pushing angle between $-\alpha/2$ and

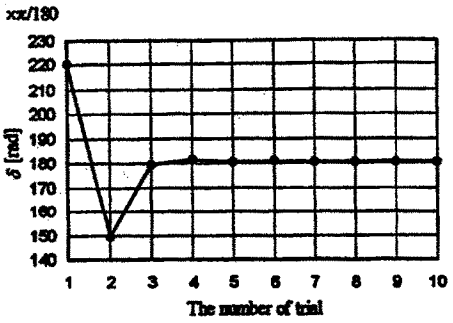

(a) δ versus the number of trial.

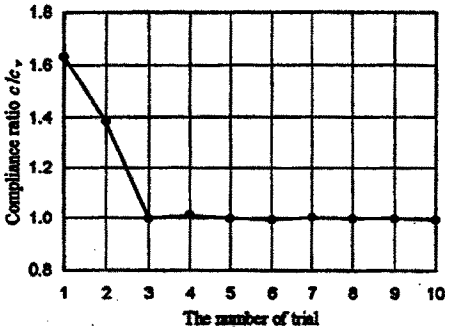

(b) c/c_ν versus the number of trial.

Figure 10. Convergence process for δ and c/c_ν.

$\alpha/2$, which supports our analytical result.

4.6. Convergence process by experiment

Fig. 10 (a) and (b) show the process of convergence of δ and c/c_ν with respect to the number of trial, respectively. It should be noted that both δ and c/c_ν converges very quickly as the number of trial increases. With three times trials, both δ and c/c_ν almost reach their equilibrium points. When c/c_ν is equal to unity, we can obtain the contact distance very accurately.

Fig.11 shows the relationship between i-th pushing direction and the direction of i-th contact force. For the first pushing, the antenna makes a lateral slip toward the left side, and for the second one, it again results in failure in avoiding a lateral slip and as a result it moves toward the right side. The third pushing direction computed by eq.(7) provides nearly the inner normal direction, and, therefore, the direction of contact force is also very close to the outer normal direction.

5. Future Works

In this work, we did not consider the effect of the curvature of the environment where the antenna makes contact. The curvature will more or less affect on the sensing accuracy. In our future works, we will address this problem in some details.

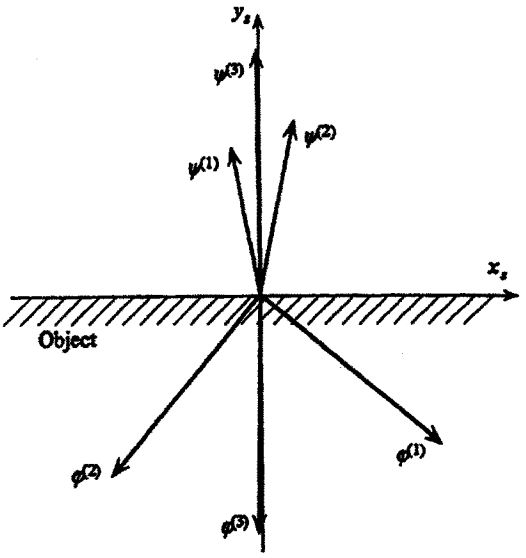

Figure 11. The relationship between $\varphi^{(i)}$ and $\psi^{(i)}$.

Finally, we would like to express our sincere thanks to Dr. Ivan Godler, Harmonic Drive Systems Co. Ltd. for his support in designing the hardware of 3D Active Antenna.

References

[1] Kaneko, M: Active Antenna, Proc. of the 1994 IEEE Int. Conf. on Robotics and Automation, pp2665-2671, 1994.

[2] Kaneko, M., N. Ueno, and T. Tsuji: Active Antenna (Basic Working Principle) Proc. of the 1994 IEEE Int. Conf. on intelligent Robotics and Systems, pp1744-1750, 1994.

[3] Kaneko, M., N. Kanayama, and T. Tsuji: 3D Active Antenna for Contact Sensing, Proc. of the 1995 IEEE Int. Conf. on Robotics and Automation, pp1113-1119, 1995.

[4] Russell, R. A.: Closing the sensor-computer-robot control loop, Robotics Age, April, pp15-20, 1984.

[5] Wang, S. S. M., and P. M. Will: Sensors for computer controlled mechanical assembly, The Industrial Robot, March, pp9-18, 1978.

[6] McKerrow, P.: Introduction to Robotics, Addison-Wesley, 1990.

[7] Brooks, R. A.: A robot that walks; Emergent behaviors from a carefully evolved network, Neural Computation, vol.1, pp253-262, 1989.

[8] Hirose, S., et. al.: Titan III: A quadruped walking vehicle, Proc. of the Second Int. Symp. on Robotics Research, MIT Pres.

[9] Schiebel, E. N., H. R. Busby, K. J. Waldron: Design of a mechanical proximity sensor, Robotica, vol.4, pp221-ss7, 1986.

[10] Russell, R. A.: Using tactile whiskers to measure surface contours, Proc. of the 1992 IEEE Int. Conf. on Robotics and Automation, pp1295-1300, 1992.